http://dx.doi.org/10.21577/0103-5053.20180179

J. Braz. Chem. Soc., Vol. 30, No. 2, 310-317, 2019
Printed in Brazil - ©2019 Sociedade Brasileira de Química

Article

Controlled Dehydration of $Fe(OH)_3$ to Fe_2O_3: Developing Mesopores with Complexing Iron Species for the Adsorption of β-Lactam Antibiotics

Paula S. Pinto,[a] Giovani D. Lanza,[a] José D. Ardisson[b] and Rochel M. Lago[*,a]*

[a]*Departamento de Química, Universidade Federal de Minas Gerais, 31270-901 Belo Horizonte-MG, Brazil*

[b]*Laboratório de Física Aplicada, Centro de Desenvolvimento da Tecnologia Nuclear (CDTN/CNEN), 31270-901 Belo Horizonte-MG, Brazil*

In this work, efficient adsorbents for β-lactam antibiotics based on mesoporous iron oxide containing surface $[FeO_x(OH)_y]$ sites were produced by controlled precipitation of iron hydroxide and thermal treatment at 150, 200, 300 and 450 °C (150FeOH, 200FeOH, 300FeOH and 450FeOH, respectively). Mössbauer, X-ray diffraction (XRD), thermogravimetry-mass spectrometry (TG-MS), Fourier transform infrared spectroscopy (FTIR), Raman, Brunauer-Emmett-Teller method (BET), scanning electron microscopy (SEM) and elemental analyses showed that the temperature caused a gradual dehydroxylation process with a significant increase of the mesoporous surface area (e.g., 114-142 $m^2\ g^{-1}$ with 46-59% mesopores, i.e., 0.04-0.09 $cm^3\ g^{-1}$) and approximate compositions of $FeO_{1.06}(OH)_{0.89}$ for 150FeOH up to $FeO_{1.38}(OH)_{0.26}$ for 450FeOH. The material 150FeOH showed high adsorption capacities of ca. 42 and 58 mg g^{-1} for amoxicillin and ceftriaxone, respectively. Experiments assessing the effect of NO_3^-, Cl^-, competitive PO_4^{3-} adsorption and H_2O_2 decomposition suggest that the $[FeO_x(OH)_y]$ surface sites located in the mesopores are involved in the efficient adsorption by complexation of the β-lactam antibiotics.

Keywords: iron oxyhydroxide, amoxicillin, adsorption, complexation, β-lactam

Introduction

Antibiotics have been widely used in human and veterinary medicine for several decades.[1,2] The β-lactams, the most varied and used antibiotics in the world,[1] contaminate the environment by different ways, e.g., excretion, industrial wastewater, inadequate drug disposal in landfills and in sewage network.[3] As these antibiotics are persistent and not efficiently degraded by conventional wastewater treatments[3-5] they may disturb the microbial communities and also can cause an increase of the resistance of pathogenic microorganisms.[6,7] Several studies have been carried out on the development of technologies to remove these antibiotics such as the use of microorganisms,[8] anodic oxidation,[9] the Fenton process,[10] photocatalysis[11,12] and ozonization.[13] Adsorption has also been used as an effective and simple alternative and materials such as wheat grains,[14] organoclays,[15,16] and chitosan based material,[17] which are some examples of adsorbents used for amoxicillin removal. Carbon-based materials, such as activated carbon,[18-20] magnetic multi-walled carbon nanotube,[21] magnetic activated carbon,[17] carbon nanofibers,[22] graphene-based materials,[23] carbon nanotubes[24,25] and graphene oxide[26] have been extensively investigated for the antibiotic adsorption. However, several of these works suggest that the relatively large β-lactam antibiotic molecules do not effectively access the narrow micropores of activated carbons.[27-29]

Recent works showed high efficiencies of Fe oxides, i.e., Fe_2O_3 supported on Al_2O_3[30] and in the waste red mud[31] for the adsorption of β-lactam molecules from water. Although a possible β-lactam complexation with iron[32] has been suggested during adsorption, the presence of support, i.e., silica, alumina and other impurities, does not allow a clear conclusion on the interaction of the antibiotic with superficial Fe^{3+} sites. Also, Ghauch *et al.*[33] suggested that β-lactam antibiotics can be adsorbed on iron corrosion products like iron hydroxides.

In this work, a controlled synthesis based on the gradual dehydroxylation of Fe hydroxide to produce a mesoporous adsorbent containing $[FeO_x(OH)_y]$ surface sites was designed to produce efficient adsorbents for β-lactam antibiotics on aqueous solutions.

*e-mail: rochel@ufmg.br

Experimental

Synthesis of the materials

The materials were prepared using a $Fe(NO_3)_3.9H_2O$ solution (50 g L^{-1}) and adding dropwise 1 mol L^{-1} NH_4OH to reach pH ca. 9. The obtained solid was filtered and washed with 10 mL of 1 mol L^{-1} NH_4OH and dried at 80 °C for 24 h. The material, FeOH, was then treated at different temperatures (150, 200, 300 and 450 °C) for 180 min in a tubular furnace in air atmosphere. The adsorbents were named as 150FeOH, 200FeOH, 300FeOH and 450FeOH, respectively.

Adsorbent characterization

The crystal structure and phase identification were obtained by Mössbauer spectroscopy (^{57}Co source in an Rh matrix using α-Fe as reference spectrum at room temperature) and powder X-ray diffraction (XRD, Shimadzu XRD-7000, Cu radiation). The composition and structure were studied by infrared (PerkinElmer FTIR GX, KBr pellet) and Raman spectroscopy (SENTERRA, 633 nm, 2 mW laser). The superficial area (Brunauer-Emmett-Teller (BET) method) and pore structure were obtained by using N_2 adsorption-desorption measurements (Quantachrome Autosorb-1). The thermal decomposition (TG) was carried out under argon with a heating rate of 5 °C min^{-1} up to 500 °C (thermobalance NETZSCH STA 449 F3) and the thermal products were analyzed by a coupled mass spectrometer (MS) NETZSCH Aëolos QMS 403C. The particle morphology was characterized by using scanning electron microscopy (SEM, FEI Quanta 200 FEI and Quanta FEG 3D FEI microscopes). The %H was obtained by elemental analysis (PerkinElmer CHN-PE-2400). Zeta potential measurements using 0.5 mg mL^{-1} of the adsorbent were conducted by the Zetasizer Nano ZS Malvern Instruments.

Adsorption experiments

The adsorption experiments were conducted using 20 mg of adsorbent and 20 mL of the antibiotic solution (100 ppm, pH 5). The removal was monitored by the maximum adsorption at 272 nm, for amoxicillin (AMX), and at 262 nm, for ceftriaxone, on UV-Vis spectrophotometer (Shimadzu UV-2550), after 24 h of contact.

The adsorption isotherms were adjusted using the Langmuir and Freundlich isotherm models and initial concentrations of amoxicillin as 25, 50, 75, 100, 150, 200, 250, 300, 350 and 450 mg L^{-1}. The pH effect (3, 5, 7, 9, 11), ionic strength (0.01, 0.1, 0.2 mol L^{-1} NaCl and $NaNO_3$) were evaluated in this study for the 150FeOH.

Furthermore, the competitive adsorption using phosphate (0.01, 0.1, 0.2 mol L^{-1}) and the H_2O_2 decomposition in the presence and absence of AMX (200 mg L^{-1})[30] were evaluated for the 150FeOH material.

Results and Discussion

Sample characterization

The different materials used in this work were prepared by a precipitation of Fe hydroxide followed by thermal treatment at 150, 200, 300 and 450 °C for the controlled dehydroxylation to produce mesopores and surface $[FeO_x(OH)_y]$ sites (equation 1):

$$Fe(OH)_3 \rightarrow FeO_x(OH)_y(\text{mesopores}) + H_2O \quad (1)$$

These samples were named hereon as FeOH (Fe hydroxide precipitate without any thermal treatment), 150FeOH, 200FeOH, 300FeOH and 450FeOH. The Mössbauer spectra at room temperature for the samples (Figure 1) indicated an amorphous superparamagnetic Fe^{3+} phase, probably related to iron hydroxide, for the materials FeOH (without thermal treatment) and 150FeOH. The thermal treatment at 200 °C led to the partial formation

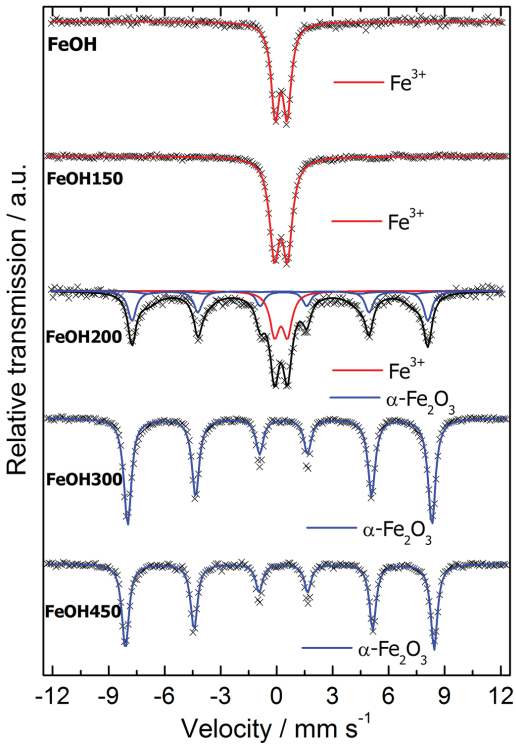

Figure 1. Mössbauer spectra for the samples FeOH and 150FeOH to 450FeOH.

of hematite α-Fe_2O_3. On the other hand, for the materials treated at 300 and 450 °C, the amorphous iron hydroxide was completely converted to hematite. Similar results have been observed before.[30,34]

XRD analyses for the samples FeOH and 150FeOH also indicated the presence of an amorphous material (Figure 2). For the materials treated at temperatures higher than 150 °C, it was observed the presence of hematite with well defined peaks at 24, 33, 36, 41, 49, 54, 57, 62, 64° (PDF 24-72). As the temperature increased, the hematite peaks became more intense and narrow, suggesting an increase in the crystallinity. The crystallite average size of α-Fe_2O_3, estimated by the Scherrer equation, varied from 12 nm for 200FeOH to 16 and 18 nm for 300FeOH and 450FeOH, respectively.

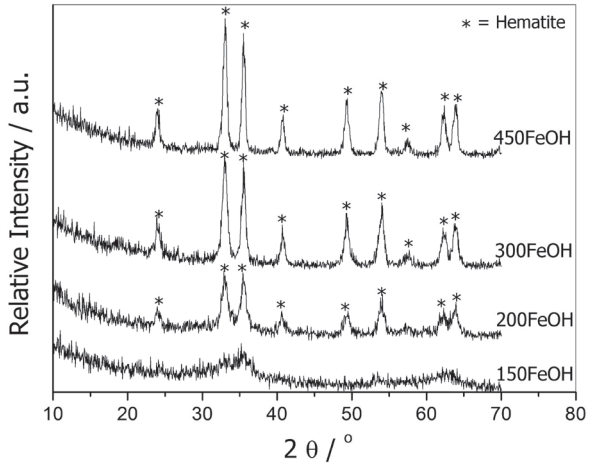

Figure 2. XRD powder diffraction for FeOH, 150FeOH, 200FeOH, 300FeOH and 450FeOH.

Raman spectra of the samples FeOH, 150FeOH and 200FeOH also suggested the formation of hematite with bands near 226, 245, 292, 410, 494 and 611 cm^{-1},[34] which became more intense at higher temperatures, i.e., 300FeOH and 450FeOH (Figure 3).

Infrared spectra (Figure 4) for FeOH and 150FeOH materials showed two broad bands related to νOH from iron species and adsorbed water in region 1, near 3402 and 3152 cm^{-1}. As the thermal treatment increased to 200, 300 and 450 °C, these bands gradually decreased, indicating a dehydration/dehydroxylation of the iron oxyhydroxy species.[35] The same was observed in region 2 for the band assigned to δH_2O between 1618-1628 cm^{-1}.[35] Simultaneously to the dehydration/dehydroxylation process, typical bands of Fe_2O_3 at 447 and 535 cm^{-1} (region 3) gradually appeared.[34]

SEM images of the FeOH suggested an agglomerated material composed of irregular particles (Figure 5). For the thermally treated materials, 150-450FeOH, no significant

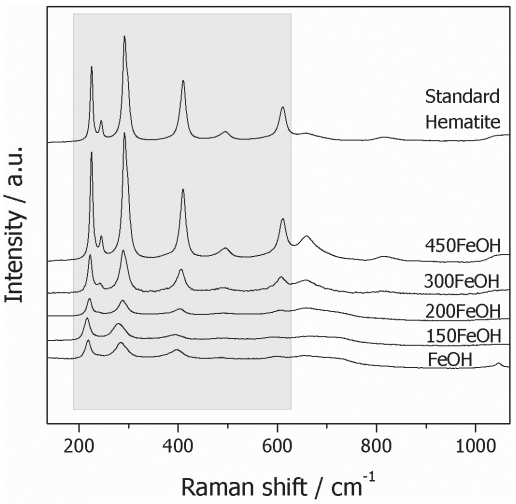

Figure 3. Raman spectra for FeOH, 150FeOH, 200FeOH, 300FeOH and 450FeOH and standard hematite.

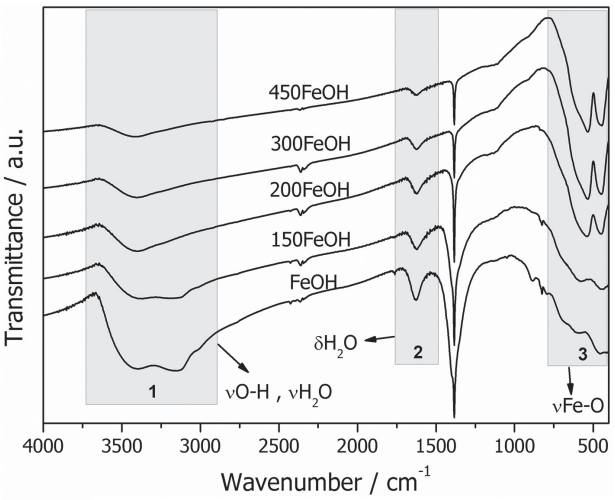

Figure 4. FTIR spectra of FeOH, 150FeOH, 200FeOH, 300FeOH and 450FeOH.

changes in the morphology was observed, except the formation of some porous structure present on the particles surfaces.

The surface area obtained by N_2 adsorption/desorption (BET method) for the 150FeOH sample was 114 $m^2 g^{-1}$ with ca. 0.04 $cm^3 g^{-1}$ (46%) of mesopores (Figure 6). Thermal treatment at 200 °C (200FeOH) led to an increase in the surface area to 142 $m^2 g^{-1}$ and mesoporosity of 0.087 $cm^3 g^{-1}$ (59%), probably due to the dehydration of iron oxyhydroxide. When the temperature was increased to 300 and 450 °C, the BET surface area decreased to 102 $m^2 g^{-1}$ (0.05 $cm^3 g^{-1}$ or 54% of mesopores) and 31 $m^2 g^{-1}$ (0.03 $cm^3 g^{-1}$ or 69% of mesopores), respectively, probably due to sintering and loss of micro and mesoporosity of the materials. These results are likely related to the conversion of the Fe hydroxide to Fe_2O_3, which at low temperatures led to the development of micro and mesoporosities, but

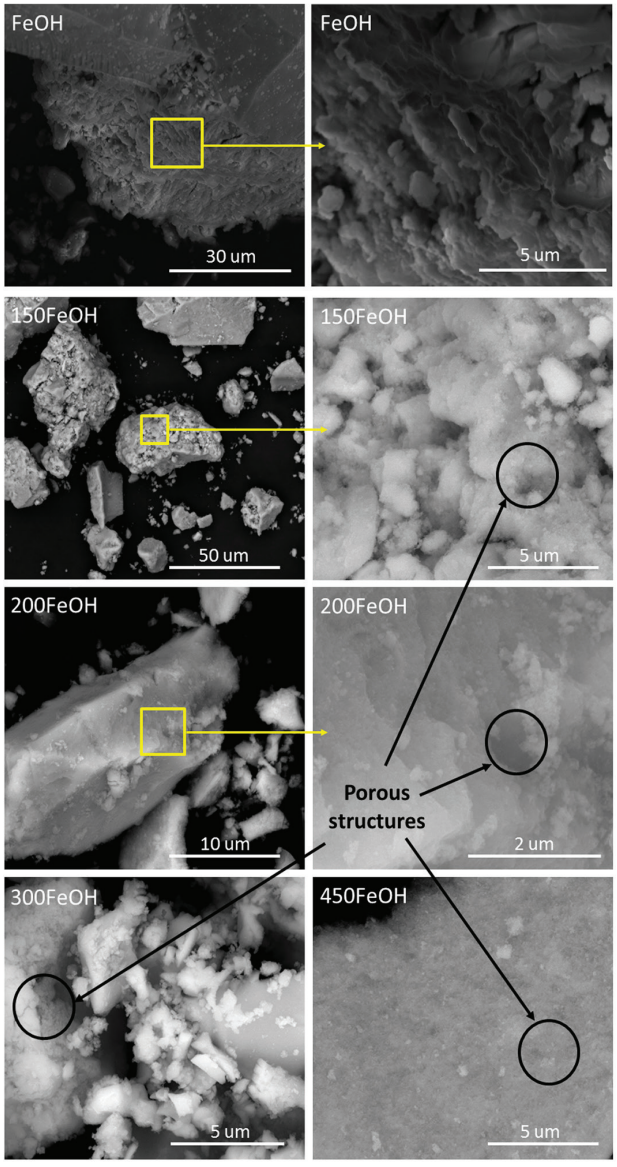

Figure 5. SEM images of FeOH, 150FeOH, 200FeOH, 300FeOH and 450FeOH samples.

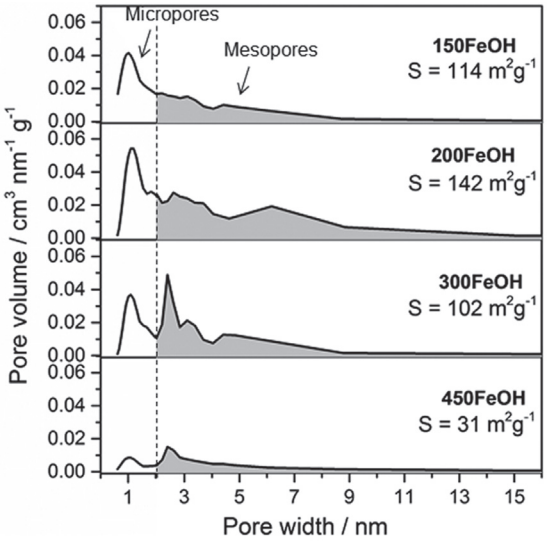

Figure 6. Pore size distribution of the materials 150FeOH, 200FeOH, 300FeOH and 450FeOH.

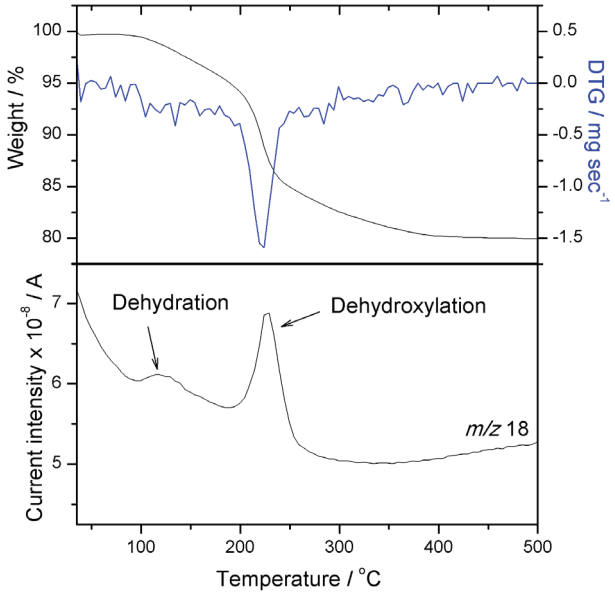

Figure 7. TGMS for the FeOH sample.

sintered at higher temperatures with a decrease on the surface area.[30,36]

The zero charge points found by zeta potential measurements were 8.0, 7.0, 7.4 and 6.8 for the samples 150FeOH, 200FeOH, 300FeOH and 450FeOH, respectively (Figure S1, Supplementary Information (SI) section).

The TGMS curves for the FeOH sample (Figure 7) showed two endothermic events related to the water loss between 100 and 200, and at 234 °C. These losses, especially at 234 °C, are related to the dehydroxylation processes. Based on %H (obtained by CHN) and TG of the different materials, the following empirical formulae were obtained for the FeOH sample treated at 150, 200, 300 and 450 °C: $FeO_{1.06}(OH)_{0.89}$ (150FeOH), $FeO_{1.21}(OH)_{0.59}$ (200FeOH), $FeO_{1.38}(OH)_{0.26}$ (300FeOH), $FeO_{1.43}(OH)_{0.14}$ (450FeOH), respectively.

β-Lactam antibiotics adsorption

The obtained materials were tested for the adsorption of the β-lactam antibiotics, amoxicillin and ceftriaxone (Figure 8). The FeOH sample showed a significant Fe^{3+} leaching and it was not possible to carry out adsorption experiments.

The best material for β-lactam antibiotics adsorption was 150FeOH, with adsorption capacity of ca. 42 and 57 mg g^{-1} for amoxicillin and ceftriaxone, respectively. A slight decrease was observed for the material treated

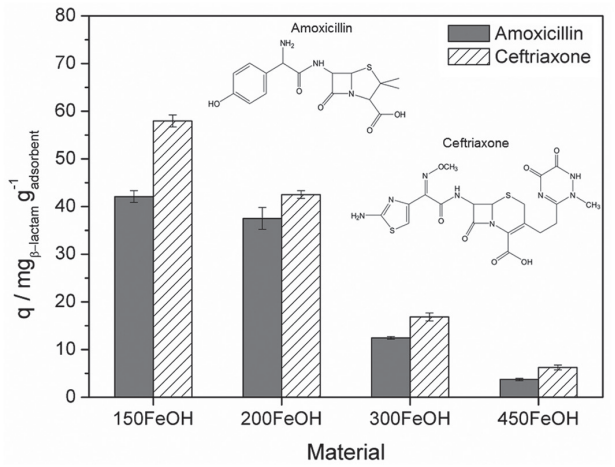

Figure 8. Adsorption of amoxicillin and ceftriaxone on 150FeOH, 200FeOH, 300FeOH and 450FeOH.

at 200 °C (200FeOH) with adsorption capacity reaching values of 38 and 43 mg g^{-1} for amoxicillin and ceftriaxone, respectively. As the thermal treatment increased to 300 and 450 °C (300FeOH and 450FeOH), a strong decrease in the adsorption capacity was observed for both antibiotics. The UV-Vis spectra of the β-lactam antibiotics after all adsorptions did not show any change, indicating that the antibiotic molecules are stable under the experimental conditions.

The amoxicillin adsorption isotherm (Figure S2, SI section) for the sample 150FeOH showed the best fit for the Langmuir model (coefficient of determination (R^2) = 0.9935) compared to Freündlich (R^2 = 0.9827), with maximum monolayer adsorption capacity of 64 mg g^{-1}, which was close to the experimental data (60 mg g^{-1}).

The effect of ionic strength was studied using NaCl and $NaNO_3$ solutions (Figure 9). It was possible to observe a decrease in the AMX adsorption capacities when 0.01-0.2 mol L^{-1} NaCl and $NaNO_3$ solutions were used.

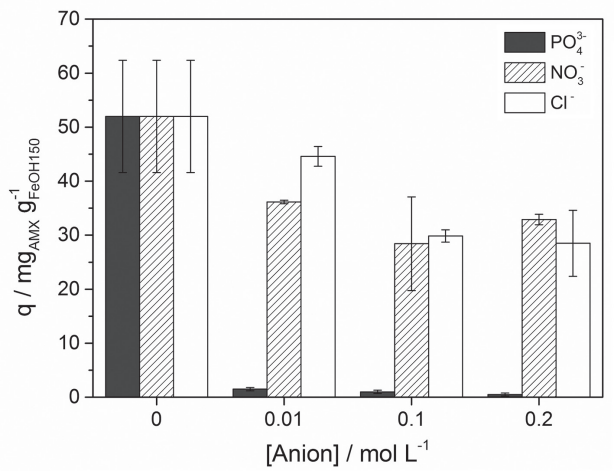

Figure 9. Effect of chloride, nitrate and phosphate on the AMX adsorption on 150FeOH.

A similar effect of salts, e.g., KNO_3, causing a slight decrease in AMX adsorption has been observed for graphene and it was discussed in terms of electrostatic interactions.[37] On the other hand, in this work, the presence of phosphate in the same concentrations caused a remarkable decrease on AMX adsorption to ca. 0.5 mg g^{-1}. This result is likely related to the strong complexation of PO_4^{3-} species to iron,[38,39] which is hindering the interaction of AMX with the surface.

The peroxide decomposition was investigated as a probe reaction to detect Fe^{3+} species available on the surface as the H_2O_2 molecule decomposes by initial complexation with Fe^{3+}_{surf}. Kinetic data of the H_2O_2 decomposition showed a linear behavior between 5 and 30 min (Figure S3, SI section), suggesting a pseudo-zero order kinetics. Figure 10 shows the H_2O_2 decomposition rates obtained for each sample in the absence (black) and presence (gray) of AMX.

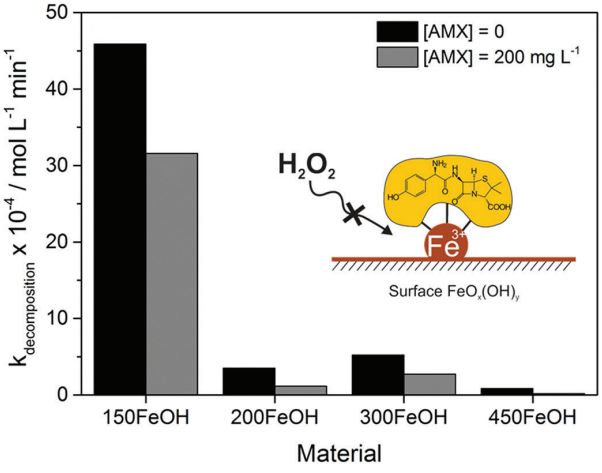

Figure 10. H_2O_2 decomposition rates in the absence (black) and presence (gray) of amoxicillin.

It can be observed in Figure 10 that the material 150FeOH was the most efficient for H_2O_2 decomposition. The treatment at higher temperature strongly decreased the peroxide decomposition. These results suggest that after thermal treatment the Fe^{3+}_{surf} available for the interaction and reaction with H_2O_2 molecules strongly decreased. Likely, dehydroxylation processes at higher temperature led to the decomposition of $[FeO_x(OH)_y]$ surface sites to form the more stable Fe_2O_3 phase. It is interesting to observe that in the presence of amoxicillin, the H_2O_2 decomposition reaction rate significantly decreased for all materials. This result, i.e., H_2O_2 decomposition inhibition by AMX, is likely due to a complexation of amoxicillin on the Fe^{3+} active site hindering the adsorption and reaction of H_2O_2 (see detail in Figure 10). Similar results have been observed in a previous work.[30]

The adsorption capacities of the FeOH produced materials were normalized by surface area and compared to other adsorbents reported in the literature for amoxicillin adsorption (Figure 11), e.g., modified red mud,[31] Fe oxide/Al_2O_3,[30] magnetic Fe_3O_4@C nanoparticle (MNPs_PAC, 671 m^2 g^{-1});[40] and modified activated carbon materials with high surface areas such as microwave-assisted KOH biochar (KAC, 1065 m^2 g^{-1}),[41] CO_2 activated carbon (OP, 1055 m^2 g^{-1}),[42] templated nanoporous carbon (TNC, 660 m^2 g^{-1}),[29] and commercial activated carbon (AC, 935 m^2 g^{-1}).[29]

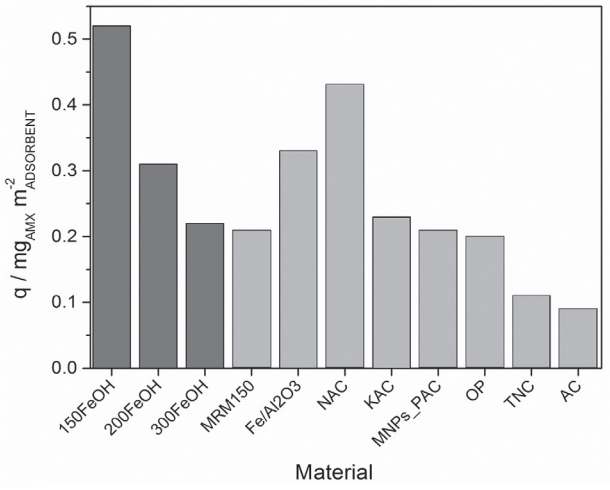

Figure 11. AMX adsorption capacities for different materials.

It can be observed a higher adsorption capacity of 150FeOH (ca. 0.52 mg_{AMX} m^{-2}) when compared to the other obtained materials in this work: ca. 0.31 and 0.22 mg_{AMX} m^{-2} for 200FeOH and 300FeOH, respectively. It is also possible to infer from Figure 11 that the 150FeOH showed higher AMX adsorption capacity under similar conditions when compared with other two classes of materials, i.e., a supported Fe oxide and carbon-based adsorbents. This result seems to indicate that the interaction of the AMX molecules with the Fe oxide surface is becoming less efficient as the materials are treated at 200 and 300 °C. This effect is likely related to the conversion of the $[FeO_x(OH)_y]$ phase to α-Fe_2O_3, which is less efficient for the antibiotic adsorption.

The results obtained in this work also seem to indicate that the adsorption of β-lactam antibiotics on Fe oxide depends on two main factors: the mesoporous surface area and the presence of surface Fe–OH labile bonds.

The material 150FeOH with the best adsorption results showed surface area of 114 m^2 g^{-1} with a good mesoporosity with a composition of $FeO_{1.06}(OH)_{0.89}$. Due to the relatively large dimensions of the AMX molecule (16 × 19 × 7 Å),[43] the presence of mesopores is very important for the adsorption process. For the sample treated at 200 °C, although the surface area increased to 142 m^2 g^{-1}, the surface labile OH species ($[FeO_x(OH)_y]$) concentration on the material strongly decreased to $FeO_{1.21}(OH)_{0.59}$, which apparently was responsible for the lower adsorption capacity. The samples 300 and 450FeOH showed both a decrease in the surface area and OH concentration leading to a further decrease in the adsorption capacity. The specific AMX adsorption (mg m^{-2}) shows a good correlation with the OH concentration (obtained from TG and CHN analyses) in the different materials (Figure S4, SI section). Moreover, the amoxicillin radius of 4.23 Å, estimated using the van der Waals volume according to Zhao *et al.*,[44] and the maximum adsorption capacity for 150FeOH, 42 mg g^{-1}, were used to estimate the area of 156 m^2 g^{-1} occupied by the amoxicillin molecules, which is fairly close to the BET value (114 m^2 g^{-1}).

These results clearly indicate that the presence of $[FeO_x(OH)_y]$ sites on the surface is important for the amoxicillin adsorption. Although the nature of the interaction of the antibiotic with the iron oxide is not clear, one can envisage a possible complexation of the AMX molecule with surface available Fe^{3+} species as suggested in previous works.[30,31] The adsorption experiments in the presence of different concentrations of NaCl and $NaNO_3$ showed a relatively low effect of ionic strength on the AMX adsorption, suggesting that ionic/electrostatic interactions have some influence on the process, but do not determine the adsorption process. On the other hand, the presence of phosphate strongly inhibited the AMX adsorption, which indirectly suggests an interaction of the AMX molecule with the coordination sphere of Fe^{3+} surface sites. Inhibition effect of AMX on the H_2O_2 decomposition also indicates a complexation of Fe^{3+} surface species. A recent experimental and theoretic work showed that AMX molecules can efficiently complex with Fe^{3+} species in aqueous medium.[32] Based on this information, it can be considered that the AMX adsorption/complexation on the iron oxide surface depends on the presence of OH labile ligands in Fe–OH species.

Figure 12 shows schematically the evolution of the Fe hydroxide to produce mesopores containing $[FeO_x(OH)_y]$ surface sites capable of complexing the AMX molecules.

Conclusions

The controlled production of a mesoporous Fe oxide phase containing surface $[FeO_x(OH)_y]$ sites resulted in efficient adsorbents for the adsorption of the hazardous β-lactam antibiotics. The results suggested that there are two effects important for the AMX adsorption: the presence of mesopores and surface $[FeO_x(OH)_y]$ species. The $[FeO_x(OH)_y]$ surface sites containing labile OH ligands

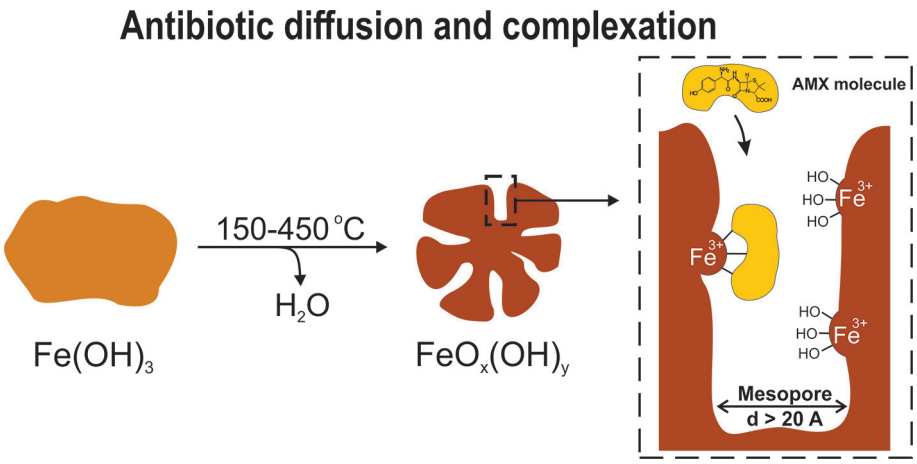

Figure 12. Schematic representation of mesopores formation by the dehydration of $Fe(OH)_3$ and AMX adsorption.

seem to be important in the adsorption process of the antibiotic molecules by complexation. These findings can be used to design new efficient materials for the adsorption of harmful antibiotic molecules.

Supplementary Information

Supplementary data (zeta potential titration of materials; adsorption isotherm of amoxicillin on 150FeOH; H_2O_2 decomposition kinetics; AMX adsorption capacity for the different [$FeO_x(OH)_y$] compositions) are available free of charge at http://jbcs.sbq.org.br as PDF file.

Acknowledgments

The authors gratefully acknowledge the financial support of the INCT MIDAS, CNPq, CAPES, FAPEMIG and UFMG Microscopy Center.

References

1. Center for Disease Dynamics, Economics & Policy (CDDEP); *State of the World's Antibiotics, 2015*; CDDEP: Washington, DC, 2015.
2. Watkinson, A. J.; Murby, E. J.; Kolpin, D. W.; Costanzo, S. D.; *Sci. Total Environ.* **2009**, *407*, 2711.
3. Homem, V.; Santos, L.; *J. Environ. Manage.* **2011**, *92*, 2304.
4. Kümmerer, K.; *Chemosphere* **2009**, *75*, 417.
5. Kümmerer, K.; *Chemosphere* **2001**, *45*, 957.
6. World Health Organization (WHO); *Antimicrobial Resistance: Global Report on Surveillance, 2014*; WHO Press: Geneva, 2014.
7. Peng, B.; Chen, L.; Que, C.; Yang, K.; Deng, F.; Deng, X.; Shi, G.; Xu, G.; Wu, M.; *Sci. Rep.* **2016**, *6*, 31920.
8. Lin, B.; Lyu, J.; Lyu, X.-j.; Yu, H.-q.; Hu, Z.; Lam, J. C. W.; Lam, P. K. S.; *J. Hazard. Mater.* **2015**, *282*, 158.
9. Giraldo, A. L.; Erazo-Erazo, E. D.; Flórez-Acosta, O. A.; Serna-Galvis, E. A.; Torres-Palma, R. A.; *Chem. Eng. J.* **2015**, *279*, 103.
10. Guo, R.; Xie, X.; Chen, J.; *Environ. Technol.* **2015**, *36*, 844.
11. Basha, S.; Barr, C.; Keane, D.; Nolan, K.; Morrissey, A.; Oelgemoller, M.; Tobin, J. M.; *Photochem. Photobiol. Sci.* **2011**, *10*, 1014.
12. Zhao, Y.; Liang, X.; Wang, Y.; Shi, H.; Liu, E.; Fan, J.; Hu, X.; *J. Colloid Interface Sci.* **2018**, *523*, 7.
13. Marcelino, R. B. P.; Leão, M. M. D.; Lago, R. M.; Amorim, C. C.; *J. Environ. Manage.* **2017**, *195*, 110.
14. Boukhelkhal, A.; Benkortbi, O.; Hamadache, M.; Ghalem, N.; Hanini, S.; Amrane, A.; *Desalin. Water Treat.* **2016**, *57*, 27035.
15. Jin, X.; Zha, S.; Li, S.; Chen, Z.; *Appl. Clay Sci.* **2014**, *102*, 196.
16. Zha, S. x.; Zhou, Y.; Jin, X.; Chen, Z.; *J. Environ. Manage.* **2013**, *129*, 569.
17. Danalıoğlu, S. T.; Bayazit, Ş. S.; Kerkez Kuyumcu, Ö.; Salam, M. A.; *J. Mol. Liq.* **2017**, *240*, 589.
18. Liu, H.; Hu, Z.; Liu, H.; Xie, H.; Lu, S.; Wang, Q.; Zhang, J.; *RSC Adv.* **2016**, *6*, 11454.
19. Sellaoui, L.; Lima, E. C.; Dotto, G. L.; Lamine, A. B.; *J. Mol. Liq.* **2017**, *234*, 375.
20. de Franco, M. A. E.; de Carvalho, C. B.; Bonetto, M. M.; Soares, R. P.; Féris, L. A.; *J. Cleaner Prod.* **2017**, *161*, 947.
21. Fazelirad, H.; Ranjbar, M.; Taher, M. A.; Sargazi, G.; *J. Ind. Eng. Chem.* **2015**, *21*, 889.
22. Li, X.; Wang, W.; Dou, J.; Gao, J.; Chen, S.; Quan, X.; Zhao, H.; *J. Water Process Eng.* **2016**, *9*, e14.
23. Wang, F.; Ma, S.; Si, Y.; Dong, L.; Wang, X.; Yao, J.; Chen, H.; Yi, Z.; Yao, W.; Xing, B.; *Carbon* **2017**, *114*, 671.
24. Chen, B.; Sun, W.; Wang, C.; Guo, X.; *Chem. Eng. J.* **2017**, *316*, 160.
25. Balarak, D.; Mostafapour, F.; Bazrafshan, E.; Saleh, T. A.; *Water Sci. Technol.* **2017**, *75*, 1599.

26. Rostamian, R.; Behnejad, H.; *Ecotoxicol. Environ. Saf.* **2018**, *147*, 117.
27. Teixeira, A. P. C.; Purceno, A. D.; de Paula, C. C. A.; da Silva, J. C. C.; Ardisson, J. D.; Lago, R. M.; *J. Hazard. Mater.* **2013**, *248-249*, 295.
28. Purceno, A. D.; Teixeira, A. P. C.; Souza, N. J.; Fernandez-Outon, L. E.; Ardisson, J. D.; Lago, R. M.; *J. Colloid Interface Sci.* **2012**, *379*, 84.
29. Barrera, D.; Villarroel-Rocha, J.; Tara, J.; Basaldella, E.; Sapag, K.; *Adsorption* **2014**, *20*, 967.
30. Pinto, P. S.; Medeiros, T. P. V.; Ardisson, J. D.; Lago, R. M.; *J. Hazard. Mater.* **2016**, *317*, 327.
31. Pinto, P. S.; Lanza, G. D.; Souza, M. N.; Ardisson, J. D.; Lago, R. M.; *Environ. Sci. Pollut. Res.* **2018**, *25*, 6762.
32. Norte, T. H. O.; Marcelino, R. B. P.; Moreira, R. P. L.; Binatti, I.; Starling, M. C. V. M.; Amorim, C. C.; Pereira, E. S.; Rocha, W. R.; Lago, R. M.; *J. Environ. Eng.* **2018**, *144*, 04018001.
33. Ghauch, A.; Tuqan, A.; Assi, H. A.; *Environ. Pollut.* **2009**, *157*, 1626.
34. Cornell, R. M.; Schwertmann, U.; *The Iron Oxides: Structure, Properties, Reactions, Occurences and Uses*, 2nd ed.; Wiley-VCH Verlag GmbH & Co. KGaA: Weinheim, 2004.
35. Ruan, H. D.; Frost, R. L.; Kloprogge, J. T.; *Spectrochim. Acta, Part A* **2001**, *57*, 2575.
36. Zboril, R.; Mashlan, M.; Petridis, D.; *Chem. Mater.* **2002**, *14*, 969.
37. Kerkez-Kuyumcu, Ö.; Bayazit, Ş. S.; Salam, M. A.; *J. Ind. Eng. Chem.* **2016**, *36*, 198.
38. Chitrakar, R.; Tezuka, S.; Sonoda, A.; Sakane, K.; Ooi, K.; Hirotsu, T.; *J. Colloid Interface Sci.* **2006**, *298*, 602.
39. Kim, J.; Li, W.; Philips, B. L.; Grey, C. P.; *Energy Environ. Sci.* **2011**, *4*, 4298.
40. Kakavandi, B.; Esrafili, A.; Mohseni-Bandpi, A.; Jafari, A. J.; Kalantary, R. R.; *Water Sci. Technol.* **2014**, *69*, 147.
41. Chayid, M. A.; Ahmed, M. J.; *J. Environ. Chem. Eng.* **2015**, *3*, 1592.
42. Mansouri, H.; Carmona, R. J.; Gomis-Berenguer, A.; Souissi-Najar, S.; Ouederni, A.; Ania, C. O.; *J. Colloid Interface Sci.* **2015**, *449*, 252.
43. Boles, M. O.; Girven, R. J.; Gane, P. A. C.; *Acta Crystallogr., Sect. B: Struct. Sci., Cryst. Eng. Mater.* **1978**, *34*, 461.
44. Zhao, Y. H.; Abraham, M. H.; Zissimos, A. M.; *J. Org. Chem.* **2003**, *68*, 7368.

Submitted: June 1, 2018
Published online: September 13, 2018